CHAPTER NINE

Essential Strategies for Revealing Nanoscale Protein Dynamics by Neutron Spin Echo Spectroscopy

David J.E. Callaway[1], **Zimei Bu**[1]
Department of Chemistry and Biochemistry, City College of New York, City University of New York, New York, USA
[1]Corresponding authors: e-mail address: dcallaway@ccny.cuny.edu; zbu@ccny.cuny.edu

Contents

1. Introduction 254
2. Essentials for Determining Nanoscale Protein Internal Motion 255
   2.1 Theory 255
   2.2 Partial Deuteration 258
   2.3 Activation of Nanoscale Internal Motion in NHERF1: A Specific Example 259
   2.4 A Simple Four-Point Model Shows How Selective Deuteration Can Enhance the Effects of Internal Motion 262
3. Preparation of Partially Deuterated Protein Samples for NSE Experiments 265
   3.1 Protein Expression and Purification 265
   3.2 Producing Deuterated Protein Subunit that is Contrast Matched in 100% D_2O Buffer Solution 266
   3.3 Reconstitution of the Partially Deuterated Protein Complex 267
   3.4 Exchanging the Proteins and Protein Complex into D_2O Buffer 267
4. Summary 268
References 268

Abstract

Determining the internal motions of a protein on nanosecond-to-microsecond timescales and on nanometer length scales is challenging by experimental biophysical techniques. Neutron spin echo spectroscopy (NSE) offers a unique opportunity to determine such nanoscale protein domain motions. However, the major hurdle in applying NSE to determine nanoscale protein motion is that the time and length scales of internal protein motions tend to be comparable to that of the global motions of a protein. The signals detected by NSE tend to be dominated by rigid-body translational and rotational diffusion. Using theoretical analyses, our laboratory showed that selective deuteration of a protein domain or a subunit can enhance the capability of NSE to reveal the internal motions in a protein complex. Here, we discuss the essential theoretical analysis and experimental methodology in detail. Protein nanomachines are far more complex than

Methods in Enzymology, Volume 566
ISSN 0076-6879
http://dx.doi.org/10.1016/bs.mie.2015.05.011
© 2016 Elsevier Inc.
All rights reserved.

any molecular motors that have been artificially constructed, and their skillful utilization likely represents the future of medicine. With selective deuteration, NSE will allow us to see these nanomachines in motion.

1. INTRODUCTION

Proteins MOVE! Protein dynamics is essential for protein function (Frauenfelder, Sligar, & Wolynes, 1991; Miyashita, Onuchic, & Wolynes, 2003; Shoemaker, Portman, & Wolynes, 2000). Proteins adapt their conformations through protein motions in order to bind a variety of ligands or to form signaling complexes (Boehr, Nussinov, & Wright, 2009; Daniel, Dunn, Finney, & Smith, 2003; English et al., 2006; Hammes-Schiffer & Benkovic, 2006; Mobley & Dill, 2009). An abundance of experimental and theoretical studies have shown that functionally important protein motions are hierarchical, occurring on timescales ranging from femtoseconds to longer than seconds, and on length scales from angstroms to micrometers (Daniel et al., 2003; Frauenfelder et al., 1991; Ha et al., 1999; Mukhopadhyay, Krishnan, Lemke, Lindquist, & Deniz, 2007; Palmer, 2004; Zaccai, 2000). Protein motions on picosecond to nanosecond timescales, and from 50 microsecond to millisecond timescales can typically be characterized by NMR at atomic resolution (Mittermaier & Kay, 2006). Single-molecule biophysics has allowed the dynamics of biological macromolecules to be observed on timescales from milliseconds to seconds (Deniz, Mukhopadhyay, & Lemke, 2008; English et al., 2006; Greenleaf, Woodside, & Block, 2007). However, protein motions on nanosecond-to-microsecond timescales and on nanometer length scales are difficult to access by existing experimental biophysical techniques, including NMR and single-molecule detection. Currently, there is a spatial–temporal dynamic gap, on nanosecond-to-microsecond timescales and on nanometer length scales, where we cannot effectively determine the dynamics of proteins and large protein complexes. Here, we refer to protein motions on nanosecond-to-microsecond timescales and on nanometer length scales as *nanoscale protein motions*.

Neutron spin echo spectroscopy (NSE) is unique in its capacity to determine nanoscale motions. NSE is one of the quasielastic neutron scattering techniques that measures the difference in velocities between the incident and the scattering neutrons, in order to determine the energy exchange between neutrons and the molecules with motions, thus obtaining the

dynamic information about the molecules (Bee, 1988; Higgins & Benoit, 1994). NSE employs the Larmor precession of neutron spins in a magnetic guide field as a clock to measure extremely small changes in velocities of scattering neutrons (Mezei, 1980; Mezei, Pappas, & Gutberlet, 2003), and thus enables the detection of very small energy changes in the scattering neutrons of $\delta E \sim 10^{3}$–10^{-2} μeV corresponding to nanosecond-to-microsecond dynamics. NSE thus fills an important spatial–temporal dynamic gap to determine nanoscale protein motions.

NSE thus has the potential to reveal protein domain motions because of the length scales and timescales probed by NSE. However, the major hurdle in applying NSE to determine nanoscale protein motion is that the time and length scales of internal protein motions are comparable to that of the global motions of a protein. The NSE measured correlation functions from a fully hydrogenated protein tend to be dominated by global motions of a protein (Hong et al., 2014; Farago, Li, Cornilescu, Callaway, & Bu, 2010). We have found that selective deuteration of a subunit can aid NSE to reveal effectively the internal domain motions in a reconstituted protein complex. Here, we first present a theoretical analysis, using nonequilibrium statistical mechanics, in order to reveal the advantage of selective deuteration. We also present the experimental scheme of selective deuteration, complex reconstitution, and sample preparation for NSE experiments. These theoretical, analytical and experimental schemes can be applied to determine nanoscale protein domain motions in a single protein, with selective deuteration of a protein domain or specific residues.

2. ESSENTIALS FOR DETERMINING NANOSCALE PROTEIN INTERNAL MOTION

2.1 Theory

2.1.1 Nonequilibrium Statistical Mechanics and the Mobility Tensor

NSE measures the intermediate scattering function $I(Q,t)$, which is the spatial Fourier transformation of the space–time van Hove correlation function $G(r,t)$ (Mezei, 1980),

$$I(Q,t) = \int_V G(r,t)\exp(-iQ\cdot r)dr$$

with Q the magnitude of the scattering vector, t the time, and r the position of a scattering center. The designation "intermediate" arises precisely because only one of the variables of $G(r,t)$ is Fourier transformed. Because

of the short wavelength of neutrons, NSE measures $I(Q,t)$ on nanometer to submicron length scales and can reveal the nanoscale fluctuations in a protein. NSE thus measures motions on nanometer to micron length scales, and on nanosecond to microsecond timescales (Ewen & Richter, 1997; Farago et al., 2010; Mezei, 1980).

For a protein in solution, $I(Q,t)$ can typically be fit to a single exponential in time (and is difficult to fit to more exponentials) at a given Q. A natural way to interpret the NSE data is to examine the effective diffusion constant $D_{\text{eff}}(Q)$ as a function of Q, which is determined by the normalized intermediate scattering function $I(Q,t)/I(Q,0)$:

$$\begin{aligned} \Gamma(Q) &= -\lim_{t\to 0}\frac{\partial}{\partial t}\ln\left[I(Q,t)/I(Q,0)\right] \\ D_{\text{eff}}(Q) &= \frac{\Gamma(Q)}{Q^2} \end{aligned} \tag{1}$$

where $I(Q,0)$ is the static form factor.

In order to describe the dynamics of a protein in solution, we utilize the Akcasu–Gurol approach originally developed to describe the dynamics of random coil polymers (Akcasu & Gurol, 1976), generalized to include rotational motion (Bu, Biehl, Monkenbusch, Richter, & Callaway, 2005; Callaway & Bu, 2015):

$$D_{\text{eff}}(Q) = \frac{k_{\text{B}}T}{Q^2}\frac{\sum_{\text{jl}}\left\langle b_{\text{j}}b_{\text{l}}\left(Q\cdot H^{\text{T}}_{\text{jl}}\cdot Q + L_{\text{j}}\cdot H^{\text{R}}_{\text{jl}}\cdot L_{\text{l}}\right)e^{\text{i}Q\cdot\left(r_{\text{j}}-r_{\text{l}}\right)}\right\rangle}{\sum_{\text{jl}}\left\langle b_{\text{j}}b_{\text{l}}e^{\text{i}Q\cdot\left(r_{\text{j}}-r_{\text{l}}\right)}\right\rangle} \tag{2}$$

where b_{j} is the coherent scattering length of a subunit j, H^{T} is the translational mobility tensor, H^{R} is the rotational mobility tensor, and $k_{\text{B}}T$ is the usual temperature factor. The structural coordinates of the macromolecule, taken relative to the center of friction of the protein are given by r_{j} (note that $\Sigma r_{\text{j}} = 0$). In practice, the structural coordinates can be atoms, protein domains in a multidomain protein, or subunits in a multimeric protein complex, and may be obtained from high-resolution crystallography or NMR, or from low-resolution electron microscopy and small-angle X-ray and neutron scattering (SAXS and SANS). In Eq. (2), $L_{\text{j}} = r_{\text{j}} \times Q$ is the torque vector for each coordinate. The brackets $\langle\rangle$ denote an orientational average over the vector Q. The translational mobility tensor H^{T} in Eq. (2) is defined by the velocity response $v = H^{\text{T}}F$ to an applied force F. The rotational mobility tensor H^{R} is defined by the angular velocity response $\omega = H^{\text{R}}\tau$ to an applied torque τ.

It is necessary to include the contributions from rotational diffusion when the timescale of the measurement is short enough. The relevant timescale is the inverse of the rotational diffusion constant. This constant can be estimated from the fact that globular proteins tumble in solution at frequencies close to that for rigid spheres. Such frequencies are usually determined via the *rotational correlation time* $\varphi = V\eta/k_{\mathrm{B}}T$, where V is the molecular volume, η is the viscosity of the medium, k_{B} is the Boltzmann's constant, and T is the temperature. Assuming the Stokes–Einstein relation $D_{\mathrm{R}} = k_{\mathrm{B}}T/(8\pi\eta R^3)$ for the rotational diffusion constant of a sphere with radius R, and using a spherical molecular volume $V = (4/3)\pi R^3$, one finds a relation between the rotational diffusion time $(D_{\mathrm{R}})^{-1} = 6\varphi$ and the molecular weight M_{w} of the protein at ambient temperatures:

$$(D_{\mathrm{R}})^{-1}(\text{nanoseconds}) \approx 3M_{\mathrm{w}}(\text{kiloDaltons})$$

Most multidomain proteins of interest are of order 50 kDa or greater, while the NSE Fourier time is at most only a few hundred nanoseconds. Thus, rotational diffusion must typically be considered in performing NSE experiments.

Equation (2) is valid for either rigid bodies or rigid-body subunits connected by soft spring linkers (Bu et al., 2005; Farago et al., 2010; Ho et al., 2004). For a completely flexible body, the rotational diffusion term (involving H^{R}) is absent. For a rigid body composed of N identical beads, the translational mobility tensor H^{T} is a matrix with N^2 identical 3×3 elements since H^{T} yields the same velocity response of, e.g., subunits B and C to a force applied to subunit A.

For an object with internal flexibility, the elements of the mobility tensor will not be equal, so forces applied to a given bead would result in different velocities for other beads and the body would not remain rigid. This reflects itself in an effective diffusion constant with a different Q dependence for rigid bodies or bodies with internal motion. Comparing models of the mobility tensor from Eq. (2) to experimental $D_{\mathrm{eff}}(Q)$ from NSE experiments allows one to extract the internal dynamics of a protein or protein complex (Bu et al., 2005; Bu & Callaway, 2011; Farago et al., 2010). The mobility tensor provides a direct indication of the existence of internal degrees of freedom (Bu et al., 2005; Bu & Callaway, 2011; Farago et al., 2010). The relationship between force, velocity, and the translational mobility tensor is illustrated in Fig. 1. These considerations allow a wide variety of results to be easily derived, such as the fact that $D_{\mathrm{eff}}(Q)$ at infinite Q is twice its value

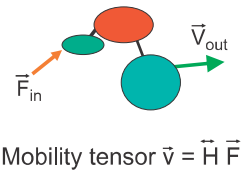

Figure 1 The relationship between force and the mobility tensor. The translational mobility tensor gives the velocity response (speed and direction) of a given protein domain to a force applied to itself or to another domain.

at zero Q for a uniform rigid body (Callaway, Farago, & Bu, 2013; Farago et al., 2010).

The above simple theoretical approach does not require complicated molecular dynamics simulations, elastic network models, fits to rotational expansions in spherical harmonics, or Navier–Stokes hydrodynamics. We do not have to fit NSE data, but can directly predict the outcome of an NSE experiment from the structural coordinates in order to test models of the mobility tensor.

2.2 Partial Deuteration

Why does partial deuteration of a protein complex enhance the ability of NSE to reveal internal motions? Initially, this seems counterintuitive, as one is using contrast variation to eliminate the scattering signal from some of the sample, and one expects naively that a smaller sample should evince a smaller signal. But one must remember that one is observing the effective diffusion constant, as per Eq. (2), and not merely the total scattering cross-section.

The partial deuteration affects $D_{\text{eff}}(Q)$ in two ways. To see this, consider the following *gedanken* experiment: Take a uniform disk and fix its center. At zero Q the effective diffusion constant $D_{\text{eff}}(Q=0)=0$, since rotational diffusion is absent because $\boldsymbol{\Sigma}\mathbf{r}=0$, and translational diffusion is absent because the center of the disk is fixed. Now deuterate half the disk and employ contrast matching to render this half invisible. Both translational and rotational diffusion (as seen by NSE) now appear at $Q=0$ because the coherent scattering length is no longer uniform and both therefore contribute to D_{eff}. Thus, D_{eff} is actually *larger* in the partially deuterated contrast matched case, since $\boldsymbol{\Sigma}(b\mathbf{r})$ is nonzero and depends on time, even though $\boldsymbol{\Sigma}\mathbf{r}=0$ and is independent of time because the center of the disk is fixed. Thus, even for a rigid body, partial deuteration increases the value of the NSE measured diffusion

constant $D_{\text{eff}}(Q)$. This effect is even more dramatic if there is internal motion, as we will see below.

Second, selective deuteration of a member of a protein complex or a protein domain can also highlight the internal modes involving hydrogenated parts of the system. From the following example, we show that partial deuteration increases the sensitivity of NSE to reveal protein internal motion.

2.3 Activation of Nanoscale Internal Motion in NHERF1: A Specific Example

NHERF1 plays essential roles in modulating the intracellular trafficking and assembly of a number of receptors and ion transport proteins. NHERF1 is a multidomain protein that has two modular domains, PDZ1, PDZ2, and a disordered but compact C-terminal domain, with three domains connected by unstructured linkers (Bhattacharya et al., 2010; Li, Dai, Jana, Callaway, & Bu, 2005; Li et al., 2007). The C-terminal domain binds to the FERM domain of Ezrin with high affinity, $K_d = 19$ nM (Reczek, Berryman, & Bretscher, 1997). We have shown that binding to FERM to the C-terminal domain of NHERF1 allosterically increases the binding affinity of both PDZ1 and PDZ2 domains of NHERF1 for the cytoplasmic tail of CFTR (Li, Callaway, & Bu, 2009; Li et al., 2005). The PDZ1 and PDZ2 domains are 110 and 80 Å away, respectively, from the FERM binding site in the CT domain. The NHERF1·FERM complex thus suggests long-range allosteric transmission of binding signals on nanometer length scales (Li et al., 2009). Our NSE experiments revealed the activation of interdomain motions of the PDZ domains in NHERF1 on submicrosecond timescales upon binding to FERM. A dynamic protein can recognize more binding partner proteins and bind to one partner more tightly than a rigid homolog (Bhattacharya et al., 2013). We thus correlate the activated domain motions with the increased binding capabilities of the PDZ domains in the complex, and thus the propagation of allosteric signals from the Ezrin-binding site to the remote PDZ domains that are located as far as 110 Å away.

For NHERF1 alone in solution, the calculated rigid body $D_{\text{eff}}(Q)$ agrees with the NSE experimental data quite well, see Fig. 2. The rigid-body calculation uses as input only the translational diffusion coefficient D_0 of NHERF1 obtained from pulsed-field gradient NMR and the "dummy atom" structural coordinates (Svergun, 1999) reconstructed from solution SAXS and SANS (Li et al., 2007, 2009).

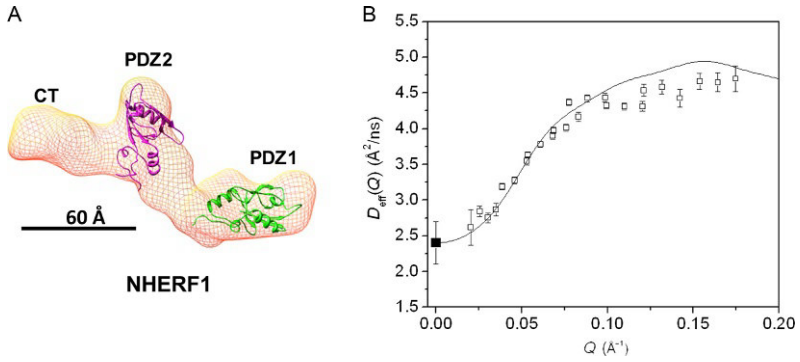

Figure 2 NHERF1 alone behaves as a rigid-body in solution as shown from NSE experiments. (A) The 3-D shape of NHERF1 reconstructed from SAXS (Li et al., 2009) using the *ab initio* program DAMMIN (Svergun, 1999). The known high-resolution structures of the PDZ1 (PDB code: 1I92) and PDZ2 (PDB code: 2KJD) domains are docked into the 3-D shape, using UCSF chimera (Pettersen et al., 2004). EBD, which overlaps with the last 13 amino acid residues that interact with PDZ2 is not marked in the graph. (B) Comparing the experimental D_{eff} (Q) of NHERF1 (black open square) with the rigid-body calculation (black solid line). The overall translational diffusion constant D_0 (filled black square) at $Q=0$ Å^{-1} is $D_0=2.4$ Å^2/ns from pulsed-PFG NMR measurements.

We have compared our calculations with the NSE experimental results on two types of complexes of NHERF1 bound to FERM, see Fig. 3. One complex is the hydrogenated NHERF1 in complex with the hydrogenated FERM (NHERF1·^{h}FERM), and the other complex is hydrogenated NHERF1 bound to deuterium labeled FERM (NHERF1·^{d}FERM). As we have pointed out that, at low Reynolds number, the dynamics of a protein as seen by NSE should not depend upon its mass, but rather upon its size. In our calculations, we thus always impose the constraint that the dynamics and therefore the mobility tensors of the hydrogenated and deuterated components are the same. When calculating $D_{eff}(Q)$ for the NHERF1·^{d}FERM complex, the scattering from the deuterated component is treated as "invisible" in Eq. (2) because of contrast matching, i.e., the neutron scattering length density of the deuterated component contrast matches that of the D_2O buffer background. We used D_0 of the deuterated complex or the hydrogenated complex obtained from PFG NMR or from dynamic light scattering and the structural coordinates obtained from SANS.

As shown in Fig. 3A, the agreement between the experimental NSE data and rigid-body calculations is poor for both the NHERF1·^{d}FERM and the

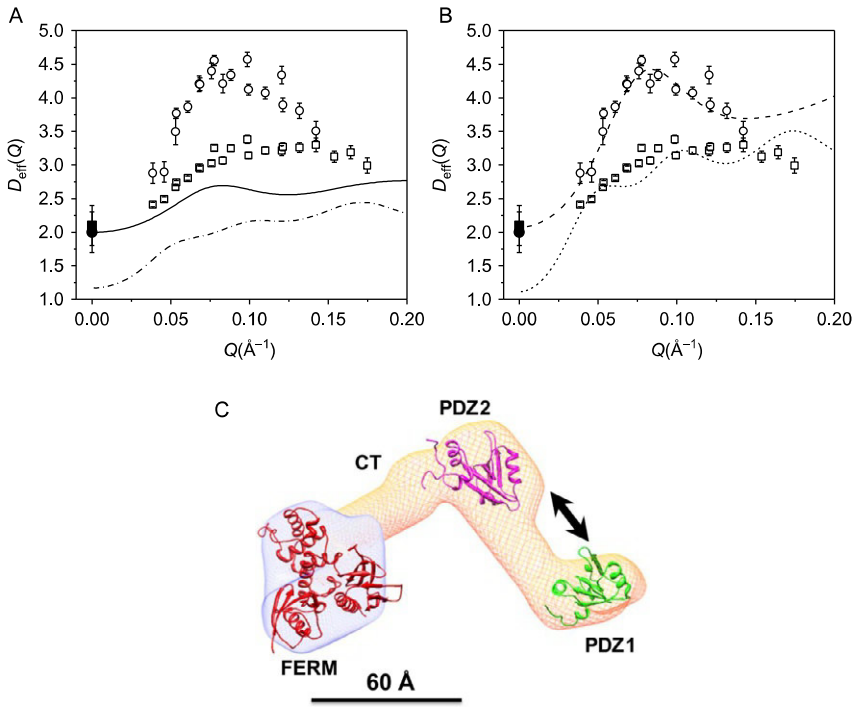

Figure 3 Activation of interdomain motion in NHERF1 upon binding to the FERM domain of Ezrin. (A) Comparing experimental $D_{eff}(Q)$ of NHERF1·dFERM and NHERF1·hFERM with rigid-body calculations. Open circle are the NSE data from NHERF1·dFERM. Open squares are the NSE data from NHERF1·hFERM. Solid circle and square are the self-diffusion constants D_0 of NHERF1·dFERM and NHERF1·hFERM obtained from PFG NMR, respectively. The solid line is from rigid-body model calculations of the NHERF1·dFERM complex. The dot dash line is from rigid-body model calculations of the NHERF1·hFERM complex. (B) Comparing experimental $D_{eff}(Q)$ of deuterated complex NHERF1·dFERM and hydrogenated complex NHERF1·hFERM with calculations incorporating interdomain motion between PDZ1 and PDZ2. The symbols for the experimental data are the same as in (A). The dashed curve is calculated from model incorporating domain motion between PDZ1 and PDZ2 for the NHERF1·dFERM complex. The short dashed curve is calculated from model incorporating domain motion between PDZ1 and PDZ2 for the NHERF1·hFERM complex. The comparisons in (A) and (B) show that deuteration of the FERM domain amplifies the effects of protein internal motions detected by NSE. (C) A model representing domain motion between PDZ1 and PDZ2 in the complex. The 3-D shape of the complex is reconstructed from SANS (Li et al., 2009). The known high-resolution structure fragments of PDZ1, PDZ2, and the FERM domain (PDB code: 1NI2) are docked into the envelope using UCSF chimera (Pettersen et al., 2004). The arrows represent translational motion between PDZ1 and PDZ2. A length-scale bar of 60 Å is shown.

NHERF1·^{h}FERM complexes. We have then incorporated domain motions in our calculations, with the mobility tensor with an internal mode between the PDZ1 and PDZ2 domains (Fig. 3B). The calculated $D_{\text{eff}}(Q)$ with internal motion agrees quite well with the NSE results for the NHERF1·^{d}FERM complex. Nevertheless, for the NHERF1·^{h}FERM complex, the computed D_0 at $Q=0$ is not close to the experimental values from PFG NMR measurements. We attribute this discrepancy to large conformational variations in NHERF1 by the unfolding of the CT domain upon binding to FERM. Such complications are minimal in the NHERF1·^{d}FERM complex because the deuterated ^{d}FERM is "invisible" to neutrons.

2.4 A Simple Four-Point Model Shows How Selective Deuteration Can Enhance the Effects of Internal Motion

The simple calculations we presented above require only the structural coordinates and a single constraint, the diffusion constant at $Q=0$ Å^{-1} for the deuterated complex, which can be measured by PFG NMR, to generate the computed $D_{\text{eff}}(Q)$. We further introduce an even more simplified model that yields the same effect, and serves to explain the $D_{\text{eff}}(Q)$ observed by NSE experiments. The simplified model is taken by extracting four points that represent the coordinates of the center-of-friction of domains obtained from the SANS data of the NHERF1·FERM complex. These points form a triangle, as shown in Fig. 4A, with the distances FERM–PDZ2 = 80 Å, PDZ2–PDZ1 = 59 Å, and FERM–PDZ1 = 110 Å. The CT domain is taken as being halfway between the FERM and PDZ2 domains. We include the point representing the FERM domain with a weight factor of three to account for its larger size relative to the other domains. Because it is possible to obtain the center-of-friction distances between the domains with confidence even with low-resolution SAXS or SANS data, this model possesses fewer uncertainties than a model based upon the molecular shape. More details of the four-point calculations are described previously (Farago et al., 2010).

Figure 4B is the $D_{\text{eff}}(Q)$ of the four-point rigid-body model, without incorporating internal domain motion between PDZ1 and the rest of the complex. Figure 4C is the $D_{\text{eff}}(Q)$ of the four-point model incorporating internal domain motion between PDZ1 and the rest of the complex. After incorporating internal motion, the overall $D_{\text{eff}}(Q)$ from the four-point model agrees well with the experimental data for both the partially deuterated and the hydrogenated complexes. The comparison between calculation and experimental data improves after including the form factor of a 20 Å

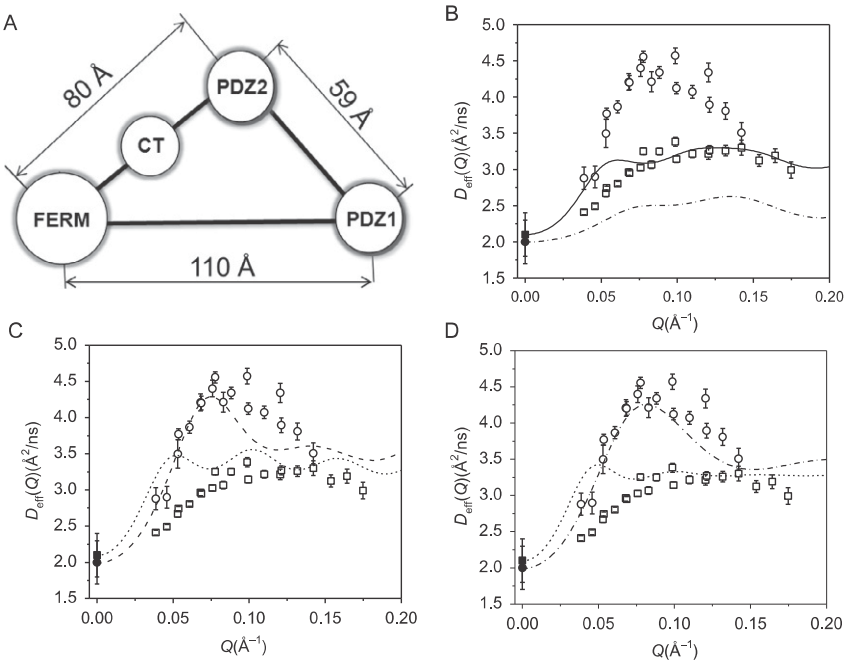

Figure 4 A simple four-point model can well describe domain motion in the complex. (A) The four-point model represents the NHERF1·FERM complex, with the centers of PDZ1, PDZ2, CT, and FERM domain taken from Fig. 3A. (B) Comparing the experimental NSE data with the four-point rigid-body calculations for NHERF1·hFERM (open squares are the experimental data and blue solid line is the calculated data) and for NHERF1·dFERM (open circles are experimental data and dot dash line is the calculated data). D_0 of NHERF1·dFERM (solid circle) squares) and NHERF1·dFERM (solid square) are from PFG NMR are shown. (C) Comparing the experimental data with calculations assuming interdomain motion between PDZ1 and PDZ2 in NHERF1·dFERM (dash line) and NHERF1·hFERM (blue (dark gray in the print version) short dash line). The experimental symbols are the same as in (B). (D) Comparing the experimental data with calculations incorporating interdomain motion between PDZ1 and PDZ2, as well as assuming finite size form factor of spheres of 20 Å radius for the FERM domain and for both PDZ domains in NHERF1·dFERM (dash dot line) and in NHERF1·hFERM (blue (dark gray in the print version) short dash line).

radius sphere for the FERM domain and both PDZ domains in the calculation (Fig. 4D). Thus, the NSE data are better represented by the four-point model that includes PDZ1–PDZ2 interdomain motion than by a model that assumes the complex is a rigid body. Further improvement likely requires the use of methods of evaluating the mobility tensors for proteins with high accuracy.

Moreover, from the four-point model calculations, we note that $D_{\text{eff}}(Q)$ for the hydrogenated rigid complex and the hydrogenated complex with internal motion are nearly indistinguishable (Fig. 5A). For the deuterated complex, $D_{\text{eff}}(Q)$ obtained from the interdomain motion model is significantly different from that of the rigid-body model (Fig. 5B). This can be explained as due to the relatively large contribution to Eq. (2) of the effects of rotational diffusion of the overall object, which dominates and obscures the effects of internal motion when no deuteration is performed. For the partially deuterated complex, both the docked domain calculation (Fig. 3B) and the four-point model (Fig. 5B) show that $D_{\text{eff}}(Q)$ of the rigid-body complex is significantly different from that of the complex with internal domain motion. Thus, deuteration of a

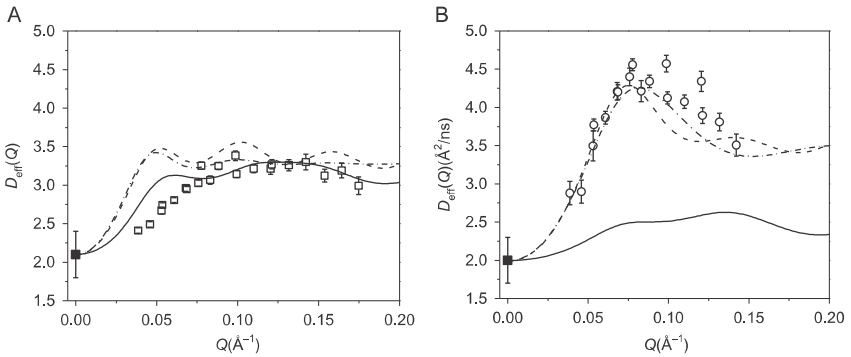

Figure 5 For the hydrogenated NHERF1·hFERM complex, the difference in $D_{\text{eff}}(Q)$ between the rigid-body model and domain-motion models is very small, but is significantly increased in the deuterated complex. (A) Comparing the rigid-body calculation with the domain-motion calculation in the four-point model in the hydrogenated NHERF1·hFERM complex. NSE data from the NHERF1·hFERM (open squares), the four-point rigid-body model (solid line), four-point model incorporating domain motion between PDZ1 and PDZ2 (dash line), four-point model incorporating domain motion between PDZ1 and PDZ2 and finite size form factor of 20 Å radius for the FERM domain, PDZ1, and PDZ2 (dash dot line). D_0 at $Q=0$ Å^{-1} as measured from PFG NMR is shown in solid square. (B) Comparing the rigid-body calculation with the domain-motion calculation in the four-point model in the deuterated NHERF1·dFERM complex. NSE data from the NHERF1·dFERM (open circles), the four-point rigid-body model (solid line), four-point model incorporating domain motion between PDZ1 and PDZ2 (dash line), four-point model incorporating domain motion between PDZ1 and PDZ2 and finite size form factor of 20 Å radius for the FERM domain, PDZ1, and PDZ2 (dash dot line). D_0 at $Q=0$ Å^{-1} as measured from PFG NMR is shown in red (light gray in the print version) solid square.

domain or subunit in a protein complex can amplify the effects of internal protein dynamics as detected by NSE.

3. PREPARATION OF PARTIALLY DEUTERATED PROTEIN SAMPLES FOR NSE EXPERIMENTS

In the discussion above, we showed that deuteration of a part of a protein or protein complex can amplify the effects of internal motion observed by NSE. Essential to this analysis is the careful preparation of deuterated proteins. The readers can refer to a thoughtful paper by Meilleur et al., which gives a comprehensive description about the methodology of deuterium labeling of proteins for neutron scattering experiments (Meilleur, Weiss, & Myles, 2009). Here, we only describe the protocol that we used to produce deuterated proteins and to reconstitute protein complexes for NSE experiments.

3.1 Protein Expression and Purification

The proteins used for our NSE experiments were all expressed in bacteria. The pET151/D-TOPO vector (Invitrogen, Inc.) or pET32a (EMD Biosciences) was used to express the FERM domain of human Ezrin (FERM, amino acid residues 1–298), the full-length human NHERF1 (residues 11–358). The protein expressed by the pET151/D-TOPO vector contains an N-terminal V5 epitope plus a hexa-histidine fusion tag. All plasmids were subjected to DNA sequencing to verify the DNA sequence.

The protein expression plasmids were transformed into Rosetta 2(DE3) cells (Novagen). The cells were grown in Luria *broth* (LB) medium until the optical density at 600 nm reaches 0.8–0.9. The cells were induced with 0.5 m*M* Isopropyl β-D-1-thiogalactopyranoside (IPTG) for 2 h. The harvested cells were resuspended and lysed in buffer containing 20 m*M* sodium phosphate buffer, 150 m*M* NaCl, 0.1 m*M* phenylmethylsulfonyl fluoride, and 10 m*M* imidazole, pH 7.5. The protein extracts were first further purified by Ni^{2+} HiTrap chelating column (Amersham Biosciences). The proteins were then purified and analyzed by size-exclusion chromatography, using a Superdex 200 10/30 column (Amersham Biosciences). The N-terminal fusion tag was cleaved using Tobacco etch virus protease (Invitrogen) after purification.

3.2 Producing Deuterated Protein Subunit that is Contrast Matched in 100% D_2O Buffer Solution

As described in Meilleur et al. (2009), proteins with 65–70% deuteration can be contrast matched in 100% D_2O. A growth medium containing 85% D_2O can usually produce proteins of 65–70% deuteration content for SANS and NSE experiments.

3.2.1 Materials

M9 medium: 4 g glucose, 0.5 g NaCl, 1 g NH_4Cl, 3 g KH_2PO_4, 3.18 g Na_2HPO_4, 2 ml of 1 *M* $MgSO_4$, 0.1 ml $CaCl_2$. The salts and glucose are dissolved in 1 l of 85% D_2O (v/v of D_2O/H_2O).

3.2.2 Procedure

The following protocol is for growing 1.0 l of cell culture. The transformed Rosetta 2 (DE3) cells are grown at 37 °C in sterile LB medium. After overnight growth, 35 ml of the cell culture is centrifuged at 5000 rpm using a table-top centrifuge. The supernatant is discarded. The cell pellet is washed in 20 ml M9 medium containing 85% D_2O (Cambridge Isotope Laboratories). The cells are pelleted by centrifugation at 3000 rpm.

The cells are then resuspended in 150 ml M9 medium containing 85% D_2O and grown at 37 °C for overnight. The $O.D._{600nm}$ of this overnight culture is about 3.5–4. The overnight culture was added to 850 ml 85% D_2O M9 medium, and the cells grow at 37 °C until $O.D._{600nm}$ reaches 0.7–0.8. This process will take about 3–5 h. The cells were then grown until $O.D._{600nm}$ reaches 0.8–0.9. The cells were then induced with 0.25 m*M* IPTG at 37 °C overnight. Protein purification and fusion tag removal for the deuterated proteins were the same as described above. After protein purification, the deuterium content of the protein is measured by MALDI-TOF to determine the exact deuterium content.

Using the above protocol, our method does not need to adapt the cells on D_2O agarose plates. This can save considerable time. However, with this method, it is important to maintain $O.D._{600nm}$ at above 0.4 after the overnight culture is added to 850 ml of 85% D_2O M9 medium. We find that it is helpful to first add the 150 ml of 85% D_2O M9 overnight culture to 500–600 ml of 85% D_2O M9 and grow the cells until the $O.D._{600nm}$ reaches 0.7–0.8. The rest of the medium is then added, and the cells are grown until the $O.D._{600nm}$ reaches 0.7–0.8 before IPTG induction.

3.3 Reconstitution of the Partially Deuterated Protein Complex

The concentration of the purified protein is measured by ultraviolet light absorbance at 280 nm, using the theoretical extinction coefficient calculated from the amino acid sequence of the protein (Gasteiger et al., 2005). The deuterated protein is then mixed with hydrogenated protein at the stoichiometry ratio of their interaction. For example, for NHERF1 binding to FERM at 1:1 molar ratio, and for CFTRct binding to NHERF1 at a 2:1 molar ratio. The protein complex is purified by size-exclusion chromatography.

The above method of using size-exclusion chromatography to separate the complex is useful to purify a protein complex with high affinity, with dissociation constant K_d from nanomolar to submicromolar. For protein complexes with weak interactions, we recommend incubating the deuterated protein at a higher molar ratio to the hydrogenated protein than the stoichiometry of the protein complex and not to use size-exclusion to resolve the complex. This is because after exchanging the protein into buffer, the deuterated component is contrast matched. NSE will measure the dynamics of the hydrogenated component in complex to the deuterated component.

3.4 Exchanging the Proteins and Protein Complex into D_2O Buffer

The protein or protein complex needs to be completely exchanged into D_2O buffer before the NSE experiment. The D_2O used for making the buffer is 99.9%. The buffer components should also be deuterated. If phosphate buffer is used, D_2O can be added to the phosphate salts, and the mixture then lyophilized. This process will be repeated for three to four times to remove the H content in the salt. If Tris buffer is used, it is recommended to use deuterated Tris, and to use DCl or NaOD to adjust the pH.

The buffer exchange uses a protein concentrating device, such as VivaSpin (Vivaproducts, Inc., Littleton, MA) with a molecular mass cutoff below the protein or protein complex. The procedures are as follows:

1. Concentrating the protein to 1/10th of original volume. Dilute the protein 10 times with D_2O buffer. Repeat the process three times.
2. Dilute the protein 10 times with D_2O buffer. Leave the solution for 12–24 h. Concentrate the protein to 1/10th volume. Add D_2O buffer to adjust the protein concentration. For our experiments, we have obtained good results with a 15–20 mg/ml protein concentration.

4. SUMMARY

We have shown that it is now possible to observe directly internal motions in proteins on nanosecond timescales and nanometer length scales. These motions have been hypothesized to be the most important dynamic modes for protein function, in long-range allostery and enzymatic catalysis. Much work remains to be done, but we are confident that our work will eliminate several formidable roadblocks to further progress. Protein nanomachines are far more complex than any molecular motors that have been artificially constructed, and their skillful utilization likely represents the future of medicine. With appropriate partial deuteration, NSE will allow us to see these nanomachines in motion.

REFERENCES

Akcasu, Z., & Gurol, H. (1976). Quasi-elastic scattering by dilute polymer-solutions. *Journal of Polymer Science, Part B: Polymer Physics*, *14*, 1–10.

Bee, M. (1988). *Quasielastic neutron scattering: Principles and applications in solid state chemistry, biology and materials science*. Bristol and Philadelphia: Adam Hilger.

Bhattacharya, S., Dai, Z., Li, J., Baxter, S., Callaway, D. J. E., Cowburn, D., et al. (2010). A conformational switch in the scaffolding protein NHERF1 controls autoinhibition and complex formation. *Journal of Biological Chemistry*, *285*, 9981–9994.

Bhattacharya, S., Ju, J. H., Orlova, N., Khajeh, J. A., Cowburn, D., & Bu, Z. (2013). Ligand-induced dynamic changes in extended PDZ domains from NHERF1. *Journal of Molecular Biology*, *425*, 2509–2528.

Boehr, D. D., Nussinov, R., & Wright, P. E. (2009). The role of dynamic conformational ensembles in biomolecular recognition. *Nature Chemical Biology*, *5*, 789–796.

Bu, Z., Biehl, R., Monkenbusch, M., Richter, D., & Callaway, D. J. (2005). Coupled protein domain motion in Taq polymerase revealed by neutron spin-echo spectroscopy. *Proceedings of the National Academy of Sciences of the United States of America*, *102*, 17646–17651.

Bu, Z., & Callaway, D. J. (2011). Proteins MOVE! Protein dynamics and long-range allostery in cell signaling. *Advances in Protein Chemistry and Structural Biology*, *83*, 163–221.

Callaway, D. J., Farago, B., & Bu, Z. (2013). Nanoscale protein dynamics: A new frontier for neutron spin echo spectroscopy. *The European Physical Journal E, Soft Matter*, *36*, 76.

Callaway, D. J., & Bu, Z. (2015). Nanoscale protein domain motion and long-range allostery in signaling proteins- a view from neutron spin echo sprectroscopy. *Biophysical Reviews*, *7*, 165–174.

Daniel, R. M., Dunn, R. V., Finney, J. L., & Smith, J. C. (2003). The role of dynamics in enzyme activity. *Annual Review of Biophysics and Biomolecular Structure*, *32*, 69–92.

Deniz, A. A., Mukhopadhyay, S., & Lemke, E. A. (2008). Single-molecule biophysics: At the interface of biology, physics and chemistry. *Journal of the Royal Society Interface*, *5*, 15–45.

English, B. P., Min, W., van Oijen, A. M., Lee, K. T., Luo, G., Sun, H., et al. (2006). Ever-fluctuating single enzyme molecules: Michaelis-Menten equation revisited. *Nature Chemical Biology*, *2*, 87–94.

Ewen, B., & Richter, D. (1997). Neutron spin echo investigations on the segmental dynamics of polymers in melts, networks and solutions. In *Neutron spin echo spectroscopy viscoelasticity, rheology. Advances in polymer science: Vol. 134* (pp. 1–129). Berlin Heidelberg: Springer. ISBN: 978-3-540-62713-5. http://dx.doi.org/10.1007/3-540-68449-2_1.

Farago, B., Li, J., Cornilescu, G., Callaway, D. J., & Bu, Z. (2010). Activation of nanoscale allosteric protein domain motion revealed by neutron spin echo spectroscopy. *Biophysical Journal*, *99*, 3473–3482.

Frauenfelder, H., Sligar, S., & Wolynes, P. (1991). The energy landscapes and motions of proteins. *Science*, *254*, 1598–1603.

Gasteiger, E., Hoogland, C., Gattiker, A., Wilkins, M. R., Appel, R. D., & Bairoch, A. (2005). Protein identification and analysis tools on the ExPASy server. In *The proteomics protocols handbook* (pp. 571–607). Springer.

Greenleaf, W. J., Woodside, M. T., & Block, S. M. (2007). High-resolution, single-molecule measurements of biomolecular motion. *Annual Review of Biophysics and Biomolecular Structure*, *36*, 171.

Ha, T., Ting, A. Y., Liang, J., Caldwell, W. B., Deniz, A. A., Chemla, D. S., et al. (1999). Single-molecule fluorescence spectroscopy of enzyme conformational dynamics and cleavage mechanism. *Proceedings of the National Academy of Sciences of the United States of America*, *96*, 893–898.

Hammes-Schiffer, S., & Benkovic, S. J. (2006). Relating protein motion to catalysis. *Annual Review of Biochemistry*, *75*, 519–541.

Higgins, J. S., & Benoit, H. C. (1994). *Polymers and neutron scattering*. Oxford: Clarendon Press.

Ho, D. L., Byrnes, W. M., Ma, W. P., Shi, Y., Callaway, D. J., & Bu, Z. (2004). Structure-specific DNA-induced conformational changes in Taq polymerase revealed by small angle neutron scattering. *Journal of Biological Chemistry*, *279*, 39146–39154.

Hong, L., Sharp, M. A., Poblete, S., Biehl, R., Zamponi, M., Szekely, N., et al. (2014). Structure and dynamics of a compact state of a multidomain protein, the mercuric ion reductase. *Biophysical Journal*, *107*, 393–400.

Li, J., Callaway, D. J., & Bu, Z. (2009). Ezrin induces long-range interdomain allostery in the scaffolding protein NHERF1. *Journal of Molecular Biology*, *392*, 166–180.

Li, J., Dai, Z., Jana, D., Callaway, D. J., & Bu, Z. (2005). Ezrin controls the macromolecular complexes formed between an adapter protein Na+/H+ exchanger regulatory factor and the cystic fibrosis transmembrane conductance regulator. *Journal of Biological Chemistry*, *280*, 37634–37643.

Li, J., Poulikakos, P. I., Dai, Z., Testa, J. R., Callaway, D. J., & Bu, Z. (2007). Protein kinase C phosphorylation disrupts Na+/H+ exchanger regulatory factor 1 autoinhibition and promotes cystic fibrosis transmembrane conductance regulator macromolecular assembly. *Journal of Biological Chemistry*, *282*, 27086–27099.

Meilleur, F., Weiss, K. L., & Myles, D. A. (2009). Deuterium labeling for neutron structure-function-dynamics analysis. *Methods in Molecular Biology*, *544*, 281–292.

Mezei, F. (1980). *The principles of neutron spin echo. Neutron spin echo: Proceedings of a Laue-Langevin Institut workshop*. Heidelberg: Springer.

Mezei, F., Pappas, C., & Gutberlet, T. (2003). *Neutron spin echo spectroscopy: Basics, trends and applications*: *Vol. 601*. Springer.

Mittermaier, A., & Kay, L. E. (2006). New tools provide new insights in NMR studies of protein dynamics. *Science*, *312*, 224–228.

Miyashita, O., Onuchic, J. N., & Wolynes, P. G. (2003). Nonlinear elasticity, proteinquakes, and the energy landscapes of functional transitions in proteins. *Proceedings of the National Academy of Sciences of the United States of America*, *100*, 12570–12575.

Mobley, D. L., & Dill, K. A. (2009). Binding of small-molecule ligands to proteins: "What you see" is not always "what you get". *Structure*, *17*, 489–498.

Mukhopadhyay, S., Krishnan, R., Lemke, E. A., Lindquist, S., & Deniz, A. A. (2007). A natively unfolded yeast prion monomer adopts an ensemble of collapsed and rapidly fluctuating structures. *Proceedings of the National Academy of Sciences of the United States of America*, *104*, 2649–2654.

Palmer, A. G., 3rd. (2004). NMR characterization of the dynamics of biomacromolecules. *Chemical Reviews*, *104*, 3623–3640.

Pettersen, E. F., Goddard, T. D., Huang, C. C., Couch, G. S., Greenblatt, D. M., Meng, E. C., et al. (2004). UCSF chimera—A visualization system for exploratory research and analysis. *Journal of Computational Chemistry*, *25*, 1605–1612.

Reczek, D., Berryman, M., & Bretscher, A. (1997). Identification of EBP50: A PDZ-containing phosphoprotein that associates with members of the ezrin-radixin-moesin family. *Journal of Cell Biology*, *139*, 169–179.

Shoemaker, B. A., Portman, J. J., & Wolynes, P. G. (2000). Speeding molecular recognition by using the folding funnel: The fly-casting mechanism. *Proceedings of the National Academy of Sciences of the United States of America*, *97*, 8868–8873.

Svergun, D. I. (1999). Restoring low resolution structure of biological macromolecules from solution scattering using simulated annealing. *Biophysical Journal*, *76*, 2879–2886.

Zaccai, G. (2000). How soft is a protein? A protein dynamics force constant measured by neutron scattering. *Science*, *288*, 1604–1607.